Molecular Therapy
Nucleic Acids
Original Article

Function Control of Anti-microRNA Oligonucleotides Using Interstrand Cross-Linked Duplexes

Yasuhiro Mie,[1] Yu Hirano,[1] Keiko Kowata,[1] Akiyoshi Nakamura,[1] Mayu Yasunaga,[2] Yoshihiro Nakajima,[2] and Yasuo Komatsu[1]

[1]Bioproduction Research Institute, National Institute of Advanced Industrial Science and Technology (AIST), 2-17-2-1 Tsukisamu-Higashi, Toyohira-ku, Sapporo 062-8517, Japan; [2]Health Research Institute, AIST, 2217-14 Hayashi-cho, Takamatsu, Kagawa 761-0395, Japan

MicroRNA (miRNA)-guided argonaute (Ago) controls gene expression upon binding to the 3′ UTR of mRNA. The miRNA function can be competitively inhibited by single-stranded anti-miRNA oligonucleotides (AMOs). In this study, we constructed a novel type of AMO flanked by interstrand cross-linked 2′-*O*-methylated RNA duplexes (CLs) that confer a stable helical conformation. Compared with other structured AMOs, AMO flanked by CLs at the 5′ and 3′ termini exhibited much higher inhibitory activity in cells. Anti-miRNA activity, nuclease resistance, and miRNA modification pattern distinctly differed according to the CL-connected positions in AMOs. Moreover, we found that the 3′-side CL improves nuclease resistance, whereas the 5′-side CL contributes to stable binding with miRNA in Ago upon interaction with the 3′ part of miRNA. These structure-function relationship analyses of AMOs provide important insights into the function control of Ago-miRNA complexes, which will be useful for basic miRNA research as well as for determining therapeutic applications of AMO.

INTRODUCTION

MicroRNA (miRNA) duplexes of 20–23 nucleotides assemble with Argonaute (Ago) family proteins, one strand (the guide strand) of which is incorporated into the miRNA-induced silencing complex (miRISC).[1,2] The Ago-loaded miRNA sequence is divided into functional parts (seed, central, supplementary, and 3′ tail) based on their roles.[3,4] The Ago-miRNA complex first recognizes target RNA through binding at the seed region and propagates pairing to the other parts. Recent research indicates that the resulting ternary complex of Ago-miRNA-target then follows one of a number of pathways: cleavage, stable, or transient binding.[5] The molecular basis for the recognition/cleavage of target RNA is currently the focus of many studies.[4–7]

MiRISCs are guided to bind to the 3′ UTRs of mRNAs and destabilize their intracellular stabilities, resulting in translational regulation. A wide variety of miRNAs are implicated in the post-transcriptional regulation of diverse cellular and developmental processes. Importantly, the expression and functions of miRNAs are also regulated by endogenous elements.[8–11] Dysregulation of miRNAs is closely related to the development or prognosis of diseases. Therefore, miRNAs are not only therapeutic targets[12–16] but also promising biomarkers.[17,18]

Anti-miRNA oligonucleotides (AMOs), or anti-miRs, bind miRNAs through complementary sequences and inhibit miRNA functions in living cells. Only seed-targeting 8-mer locked nucleic acid (LNA)-based AMOs had also reported to be effective in inhibiting miRNA.[19] Various chemical modifications of AMOs are used to improve nuclease resistance, strong affinity to target, and cellular uptake.[20] Sugar modifications, such as 2′-*O*-methyl, 2′-methoxyethyl, 2′-fluoro, or bicyclic LNA, are most commonly employed to enhance affinity to RNA targets and nuclease resistance. Biostability or pharmacokinetic properties can be improved by substituting the phosphodiester (PO) backbone linkages with phosphorothioate (PS) linkages or using peptide nucleic acid (PNA) or morpholino oligomers.[21–25] In contrast to these synthetic inhibitors, plasmid-based anti-miRNA molecules (sponges or erasers) have been also developed to continuously express the inhibitory effect after cell division.[26–30]

Although the linear single-stranded oligonucleotide form of AMOs are mainly employed, unique secondary-structured AMOs show high anti-miRNA activity.[31] In addition, double-stranded duplexes flanking the single-stranded AMO sequence improve the inhibitory effects;[32,33] however, the molecular mechanisms underlying the duplex role in AMO function is still unclear. Further studies are required to determine the roles of duplexes in maintaining the double-stranded forms, since there is a risk of dissociation into single strands. Although duplex structures are stabilized by interacting with hairpin loops, hairpin-stem-loop structures sometimes form

Received 8 July 2017; accepted 8 November 2017;
https://doi.org/10.1016/j.omtn.2017.11.003.

Correspondence: Yasuo Komatsu, Bioproduction Research Institute, National Institute of Advanced Industrial Science and Technology (AIST), 2-17-2-1 Tsukisamu-Higashi, Toyohira-ku, Sapporo 062-8517, Japan.
E-mail: komatsu-yasuo@aist.go.jp

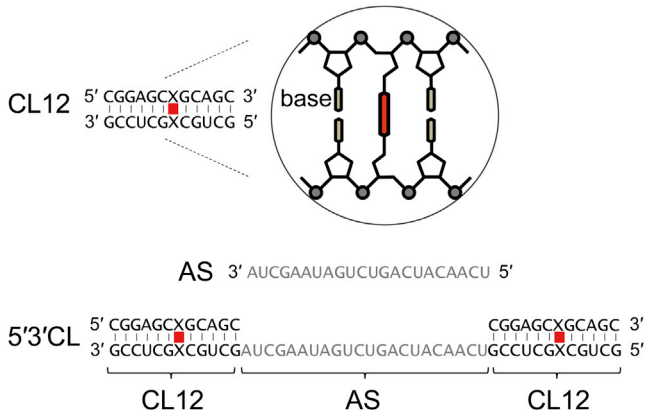

Figure 1. Sequences of Interstrand Cross-Link of 12-mer MeRNA Duplex (CL12) and Representative AMOs (AS, 5′3′CL) Targeting miR-21 Used in the Present Study

Complementary sequence to miR-21 is shown in gray. Vertical bold lines and Xs indicate the cross-linker and cross-linked sites.

concatemers upon intermolecular binding because of self-complementarity. Moreover, duplex stabilities largely depend on their sequences or molecular environment.[34]

Interstrand cross-link of DNA or RNA inhibits double strands from dissociating into single strands.[35,36] We previously developed a sequence-specific cross-link reaction that conjugates a pair of apurinic/apyrimidinic sites (AP sites) on complementary oligodeoxynucleotides (ODNs) using a short bifunctional cross-linker containing bis-aminooxy groups.[37] The cross-link formation makes the duplex rigid[38] and provides stable DNA scaffolds where enzymes are immobilized to catalyze glucose.[39] This method also enables preparation of a plasmid containing interstrand cross-links at specific sites.[40]

This paper aims to investigate the roles of duplexes flanked with the antisense in the inhibition of miRNA using the stable cross-linked duplex to reveal the structural basis of AMOs for efficient control of gene silencing. We constructed AMOs flanked by cross-linked duplexes to measure the inhibitory activity against miRNAs. AMOs containing the CLs strongly inhibited miRNA functions more efficiently than AMOs with normal single or double strand(s). Notably, the inhibitory activity largely depended on the positions of the duplex in AMO molecules. The results of the structure-function relationship not only suggest the possible interaction between the duplex domain and Ago-miRNA complex but also provide useful insights in constructing more potent AMOs.

RESULTS

Interstrand Cross-Link of a Pair of AP Sites in Double-Stranded MeRNA Stabilizes the Helical Conformation

A previous study has reported that an antisense flanked by 16- or 18-mer duplexes inhibits miRNA functions more effectively than a single-stranded one.[32] To stabilize the shorter duplex, we planned to cross-link the duplex regions with a bifunctional linker that conjugates a pair of AP sites on complementary strands.[37] To prepare AMOs from 2′-*O*-methyl RNA (MeRNA), we first examined whether AP-site cross-linking could occur in MeRNA duplexes. A MeRNA 12-mer duplex containing a deoxyuridine on each strand was treated with uracil DNA glycosylase, followed by cross-linking with a bifunctional linker (Figure S1). The MeRNA duplex cross-linked as efficiently as a DNA duplex,[37] and a cross-linked MeRNA duplex CL12 (Figure 1) was obtained. Circular dichroism (CD) analyses of CL12 revealed a spectrum with a strong positive peak at 265 nm (Figure S2A), indicating that it has a typical A-form structure similar to the perfect match for a 12-mer duplex (DS12). When the incubation temperature was gradually increased, the molecular ellipticity (ME) of CL12 remained constant at all temperatures, whereas that of DS12 drastically decreased above 65°C (Figure S2B). This result indicates that the helix conformation of CL12 can be stably maintained even under heat-denaturing conditions.

AMOs Flanked by Cross-Linked MeRNA Duplex (CL) Exhibit High Inhibitory Activity

An antisense 22-mer (AS) targeting miR-21 flanked by CL12 at both terminals was constructed to stabilize duplex domains, yielding 5′3′CL (Figures 1, S1, and S3). As control molecules, AMOs were prepared with single strands (5′3′SS), double strands (5′3′DS), and hairpin stems (5′3′HP) (Figures 2A and S3). All AMOs were independently transfected into HeLa cells at concentrations ranging from 0 to 10 nM, and inhibitory activities against miR-21 were evaluated using a dual luciferase system comprising the *Renilla* luciferase (hRluc) gene with the miR-21 binding sequence and *firefly* luciferase (Fluc) gene as an internal control (Figure 2B).[19,41] The ratios of hRluc/Fluc were normalized using the ratio from the control cells that were transfected with a dual luciferase reporter without miR-21 binding sequence. Both AS and AS flanked by single-stranded 12-mer (5′3′SS) had negligible effects on miR-21 at 48 hr after transfection. However, the AS flanked by perfect-match 12-mer duplexes (5′3′DS) showed significant inhibition. 5′3′HP with stable hairpin loops[20,32] further enhanced the efficacy, but the repression level did not reach a plateau even at 10 nM. These structural dependences are consistent with the result described in the previous report.[32] In contrast, 5′3′CL exhibited maximum activity at 5 nM and was found to have the most potent activity among other AMOs (Figure 2B). Two nucleotide mismatches in the anti-seed region (5′3′CL-M) or deletion of the sequence complementary to the 3′ half of miR-21 (5′3′CLs) significantly reduced activity (Figure 2B), indicating that both the seed and the 3′ half of the miRNA are essentially recognized by 5′3′CL. It is noted that compared with 5′3′DS or 5′3′HP, 5′3′CL has the potential to stably hybridize with the target RNA, as observed at the melting temperature (Figure 2A). This stable hybridization with the target RNA is due to the higher stacking effect of CL. A similar stabilization of the hybridization was also observed in cross-linked DNAs (Y.K., unpublished data). Notably, 5′3′CL showed significantly higher activity than a number of commercially available AMOs composed of double-stranded flanking structures (Figure S4) or single-stranded LNA-based structures (data not shown).

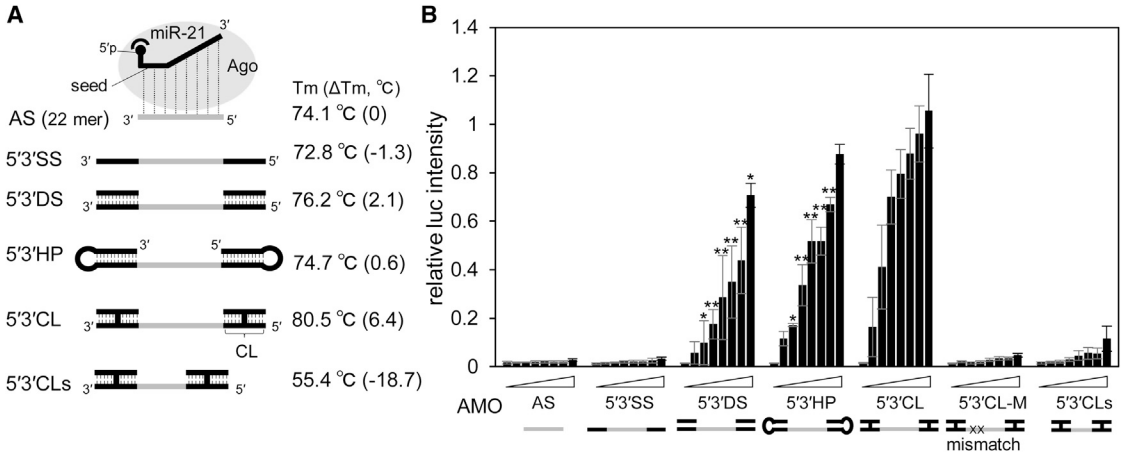

Figure 2. Inhibitory Activity Assays of AMOs Flanked by Single Strands, Double Strands, Hairpin Stems, or CL at Both Termini

(A) Schematic drawings of the secondary structure of each AMO and their Tm values in hybridizing with synthetic miR-21 RNA. Vertical bold and dotted lines indicate cross-linking and base pairing, respectively. Differences in Tm values from that of AS are indicated as ΔTm in parentheses. (B) Relative luciferase intensities in dual luciferase assays at several AMO concentrations (0, 0.5, 1, 2, 3, 4, 5, and 10 nM). Normalized intensities are represented as mean ± SD (n = 3 independent experiments). A t test was performed with 5′3′DS and 5′3′HP against 5′3′CL at the same concentrations. *p < 0.05 and **p < 0.01.

Inhibitory Activity Largely Depends on Positions of the Duplex Connected to AMO Molecules

Next, one of either the 5′ or 3′ terminal ends of the antisense was linked with four types of dangling structures (SS, DS, HP, or CL), as used in both termini-modified AMOs (Figures 3A and S3). AMOs with duplexes at the 3′ side (3′DS, 3′CL, 3′HP) did not inhibit miR-21 at concentrations from 0.5 to 5 nM (Figure 3A), and a faint signal was observed only at 10 nM of 3′CL. In contrast, AMOs with 5′-side modifications (5′CL, 5′DS, 5′HP) notably retained inhibitory activities, although those were slightly lower than that of 5′3′CL (Figure 3A). Importantly, the activity of 3′CL did not reach the level of 5′CL even at high AMO concentrations (Figure S5), in spite of the fact that there are no differences in melting temperature (Tm) values between each AMO (Figure 3A). These results suggest the possibility that 5′- and 3′-side duplexes of AMO molecules might have different modes of action in preventing miRNA function. In addition, the activities of 5′CL and 5′CLHP (cross-linked hairpin) were higher than those of their parent molecules (5′DS and 5′HP; Figure 3A), confirming that the cross-linked duplex could be an effective structure for anti-miRNA function. Together with the inactivity of 5′SS with a single strand on the 5′ side (data not shown), the dependencies on the dangling structures imply that the bulky or rigid structure on the 5′ side of AMO significantly contributes to anti-miRNA function. Lennox et al.[42] have synthesized single-stranded AMOs comprising a non-nucleotide molecule, N,N-diethyl-4-(4-nitronaphthalen-1-ylazo)-phenylamine (ZEN), at the 5′ or 3′ terminal. In that report, the 5′-ZEN-modified AMO exhibited higher anti-miRNA activity than the 3′-modified AMO, which is a trend similar to that of our results. Considering these results together, anti-miRNA activities might be largely affected by either the position or the molecular size of structures flanking the antisense region in AMOs.

MiRISC mediates degradation of mRNA through full or partial complementary binding.[43,44] Thus, the mRNA decay of the reporter hRluc gene linked to the miR-21 binding sequence (RL-miR-21bs) was examined using qRT-PCR after transfection with 5′3′CL, 5′CL, or 3′CL. The mRNA level of the RL-miR-21bs was significantly increased following transfection with AMOs (Figure S6). This result indicates that AMOs interacted with miRNA, and importantly, the increased level of the target mRNA is in good accordance with the differences in the inhibitory activities determined in the luciferase assays (5′3′CL > 5′CL > 3′CL).

Since the 5′ duplex exerted a remarkable effect on anti-miRNA activity, the positional effect of the 5′ duplex of the antisense region was further evaluated by inserting two or five nucleotides between the antisense and the 5′ duplex (5′CLsp2 and 5′CLsp5; Figure S3). As shown in Figure 3B, the anti-miRNA activities of both spacer-inserted AMOs significantly decreased compared to that of the 5′CL depending on the spacer lengths (Figure 3B). A similar reduction was observed when apparent spacers were formed at the junctions by deleting one or three nucleotides from the 5′ duplex domains (5′CLΔ1, 5′CLΔ3, and 5′CLHPΔ3; Figure S7). In contrast, the low activity of 5′CLsp2 could be restored to the same level as that of 5′CL by forming base pairs at the spacer region (5′CLsp0; Figure 3B). Note that anti-miRNA activities of the spacer-inserted AMOs are correlated with a decrease in Tm values. This is mainly derived from the diminishment of the stacking effect of the 5′-side duplex upon hybridization with miRNA. Thus, stable binding with miRNA might be one of the important factors for the high activity of 5′CL.

When 5′CL-modified-AMO (5′CL-AMO) binds to miRNA on Ago, the 5′ duplex is located proximally to the 3′ tail of miRNA. According to a previous research, the 3′ tail docks to the PAZ domain of Ago and

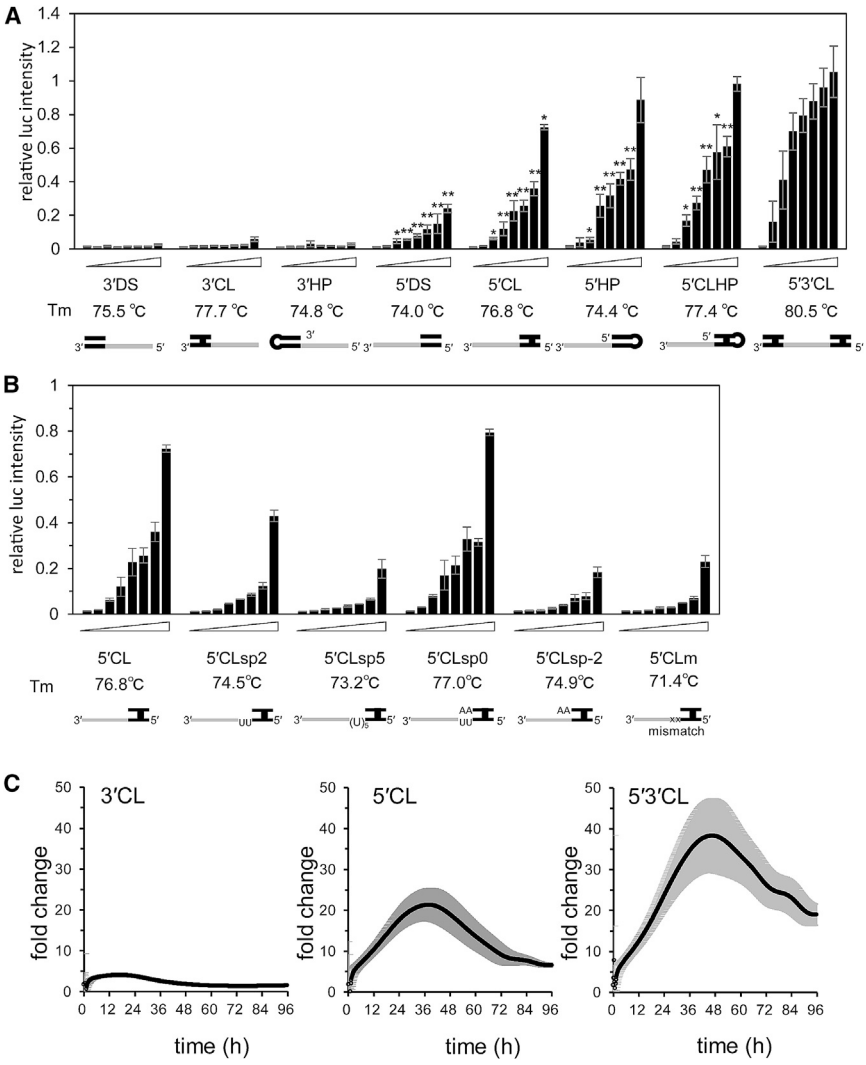

Figure 3. Inhibitory Activity of AMOs Flanked by Duplex structures at the 5′- or 3′-Terminus

Inhibitory activity of AMOs flanked by duplex structures at the 5′ or 3′ terminus (A) and AMOs having different junction structures at the 5′-side duplex (B). AMO concentrations varied from 0 to 10 nM (0, 0.5, 1, 2, 3, 4, 5, and 10 nM). Each Tm value of the AMO-miR-21 complex is indicated below the horizontal axis. Relative intensities are represented as mean ± SD (n = 3 independent experiments). A t test was performed against 5′3′CL at the same concentrations. *$p < 0.05$ and **$p < 0.01$. (C) Real-time bioluminescence monitoring of anti-miRNA activities of 3′CL, 5′CL, and 5′3′CL. 5′-CL-AMOs (5′3′CL and 5′CL) showed much higher inhibitory activities over time (approximately 96 hr) after transfection than 3′-CL-AMO (3′CL). Black and gray bars indicate average and standard deviation values, respectively, calculated from the data obtained from four replicates.

is not involved in base-paring with single-stranded target RNA.[45] To examine whether the 3′ tail binds with 5′CL-AMO, we introduced nucleotide mismatches into the 5′ end of the antisense region (5′CL-M) or masked the 3′ tail binding site using a longer strand of CL (5′CLsp-2) (Figure S3). Interestingly, the activities of both 5′CL-M and 5′CLsp-2 markedly decreased compared to 5′CL (Figure 3B). These results reveal that the 3′ tail is recognized by 5′CL-AMOs and that the 3′ tail binding is considered to be stabilized by the adjacent CL, which has a high stacking effect on hybridization at the tandem position.

The aforementioned dual luciferase assay was an endpoint evaluation. To compare inhibition kinetics, we conducted real-time bioluminescence monitoring by means of dual-color assay system, one of which contains the green-emitting luciferase gene (SLG) with the miR-21 binding sequence and the other the red-emitting luciferase gene (SLR3) as an internal control reporter, which expresses under the control of TK promoter.[46,47] After 3′CL, 5′CL, and 5′3′CL were independently transfected into HeLa cells at a concentration of 2 nM, normalized luminescence intensities of SLG by SLR3 were calculated between 0 and 96 hr (Figure 3C). While there were no signal changes following transfection with only buffer or the mismatch AMO (5′3′CL-M; data not shown), the luminescent values of 3′CL, 5′CL, and 5′3′CL increased up to 15 hr, 38 hr, and 48 hr, respectively. At maximum points, 5′3′CL and 5′CL showed 38- and 21-fold changes, respectively, whereas 3′CL only showed a 4-fold increase (Figure 3C). The differences in the inhibitory activities obtained in this real-time bioluminescence monitoring were consistent with those in the endpoint assay. Notably, 5′3′CL not only showed the highest activity at all time points but also maintained a 20-fold increase up to 96 hr post-transfection, indicating the long duration of gene silencing with this type of AMO.

Moreover, endogenous target protein level upon the transfection of AMOs in HeLa cells was analyzed. Phosphatase and tensin homolog deleted on chromosome 10 (PTEN) is known to be a target of miR-21 and a tumor suppressor.[48] The level of PTEN increased following the transfection of 5′3′CL and 5′CL, whereas no significant change was observed for 3′CL (Figure S8).

The 3′-Side CL Confers Nuclease Resistance to AMOs

Anti-miRNA activities were dependent on the CL-connected termini. To evaluate the nuclease resistance of CL-modified AMOs (CL-AMOs), 5′3′CL, 5′CL, and 3′CL were subjected to exonuclease treatment. While 5′CL was sensitive to 3′ exonuclease digestion, both 5′3′CL and 3′CL exhibited high resistance (Figure 4A). The

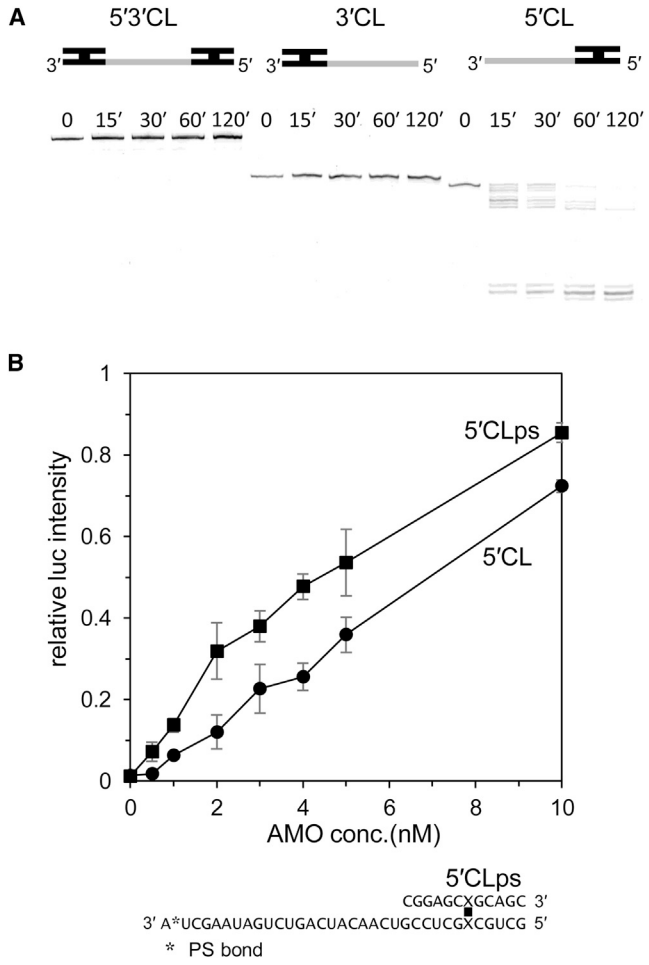

Figure 4. Nuclease Resistance of CL-AMOs

(A) Denaturing PAGE analysis of AMOs (5′3′CL, 3′CL, and 5′CL) treated with snake venom phosphodiesterase (SVPD). The number on each lane indicates the reaction time. (B) Inhibitory activity of the CL-AMO with a phosphorothioate linkage at the 3′ end. Relative luciferase intensities of 5′CL and 5′CLps were plotted versus concentrations of each AMO (0, 0.5, 1, 2, 3, 4, 5, 10 nM).

same trend was observed for human serum treatment (Figure S9). These results evidently demonstrate that the 3′-side CL protects the single-stranded antisense region from 3′-to-5′ exonuclease digestion and indicate that inactive 3′CL could be stable in cells. The nuclease lability of 5′CL raised the possibility that the anti-miRNA activity of 5′CL could be enhanced by improving its nuclease resistance. To assess this hypothesis, the 3′-terminal phosphorodiester linkage of 5′CL was modified to phosphorothioate to confer nuclease resistance (5′CLps; Figure 4B). As expected, 5′CLps exhibited an approximately 2-fold increase in miR-21 inhibition, particularly at low-AMO concentrations.

Highly Active CL-AMOs Sequester miRNAs

Next, to understand the mode of action for the CL-AMOs to inhibit miRNA activity, miR-21 was recovered from AMO-treated HeLa cells and analyzed by northern blotting with comparison to control cells. Two bands were observed on northern blotting analysis from the control cells (Figure 5A). Recently, Boele et al.[49] have reported that miR-21 is produced in two prevalent isomiR forms, miR-21 (22 nt) and miR-21 plus cytidine at the 3′ end (miR-21 + C) (23 nt). Accordingly, the upper band in the blot with lower mobility corresponds to miR-21 + C and the lower band to miR-21. With 5′3′CL and 5′CL transfections, both miR-21 + C and miR-21 were detected and were similar to those in the control cells, although miR-21 was enhanced to some extent relative to miR-21 + C (Figure 5A). On the other hand, multiple bands were observed in the 3′CL-treated cells (Figure 5A). This result is the same as that reported in the transfection with a single-stranded AMO,[50] and it has recently been revealed that nucleases and transferases mediate the 3′ end trimming and tailing of miRNA by responding to binding with a single-stranded AMO.[51] On the basis of all results, 3′CL might interact with miRNA in the same manner as a single-stranded AMO, whereas both 5′3′CL and 5′CL might suppress miRNA modification through a different way of interacting with miRNAs (see Discussion). Note that miR-21 was slightly enhanced relative to miR-21 + C in the transfection of either 5′3′CL or 5′CL compared with the control cells (Figure 5A). We speculate this change in relative levels of miR-21 and miR-21 + C may be derived from the removal of protruded cytidine residue at the 3′ end of miR-21 + C by 3′-to-5′ exonuclease. The original and 3′-trimmed miR-21 would not be further degraded in the transfection of 5′CL or 5′3′CL because the 3′ end is protected from exonuclease digestion by the neighboring 5′ side of the CL structure. Previous studies have reported that chemically modified "high-affinity" AMOs[52–54] or plasmid-based miRNA inhibitors[29,30] do not degrade miRNAs but mainly sequester them in the cells. 5′CL and 5′3′CL might suppress miRNA functions using this mechanism.

CL-AMO Structure Largely Affects Its Binding Efficiency to Ago2-RISC Complex

To investigate whether CL-AMOs function on RISC, immunoprecipitation (IP) using anti-Ago2 antibody was conducted following transfection with CL-AMOs (5′3′CL, 5′CL, and 3′CL). Each AMO could be recovered in the IP analysis, as shown in Figure 5B, demonstrating an association with Ago2-bound RISC. After 48 hr, 5′3′CL might be slightly degraded in the cells as evidenced by a faint signal detected on northern blot, moving faster in the gel from 5′3′CL. Even though the 5′- or 3′-side CL is digested by nucleases, the antisense region of 5′3′CL could remain unaffected. Next, we co-transfected cells with equivalent moles of AMOs to compare the binding ability toward Ago2-RISC complex under competitive conditions. When 5′CL was co-transfected with single-stranded AMO (5′SS; Figure S3) having very weak anti-miRNA activity (data not shown), only the 5′CL band was detected in northern blotting (Figure S10). Next, cells were co-transfected with equivalent moles of 5′CL, 3′CL, and 5′3′CL; 5′3′CL was mainly detected (Figure 5C, left lane in IP). These results are consistent with the activity observed in the luciferase assay. In co-transfection with 5′CL and 3′CL, both CL-AMOs were observed in the gel analysis, but importantly, the normalized band intensity of 5′CL was about 8-fold higher than that of 3′CL (Figure 5C, right lane

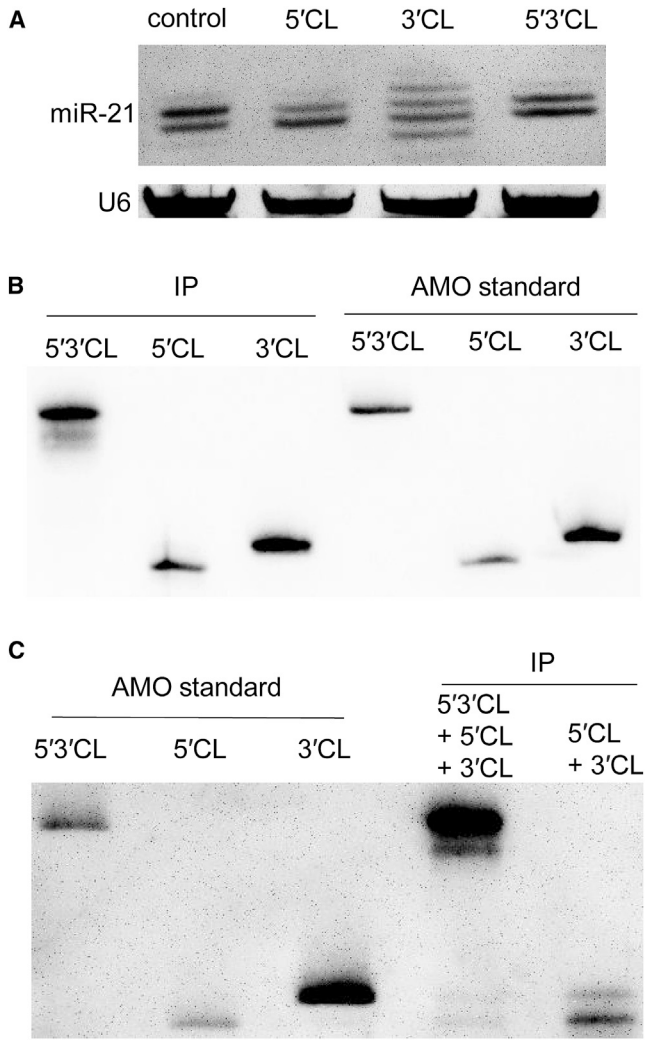

Figure 5. Analyses of miRNA and AMO after AMO Transfection

(A) Northern blot analysis of miR-21 expression level in HeLa cells transfected with 10 nM AMOs (5′3′CL, 5′CL, and 3′CL) after 48 hr. Transfection without AMO was used as control. (B and C) Analysis of AMO co-immunoprecipitated (IP) with Ago2 after transfection. Blotting images were obtained following transfection with 2 nM of each AMO (B) and with three (5′3′CL + 3′CL + 5′CL) or two (3′CL + 5′CL) AMO mixtures of 2 nM each (C).

in IP). As described above, 5′CL is more nuclease-labile than 3′CL, and there is no difference in Tm values between either CL-AMO. Therefore, this result suggests the possibility that 5′CL has potential to form a complex with RISC more effectively.

CL Effects on miRNA Inhibition Are Generally Observed

Next, we synthesized CL-AMOs targeting other miRNAs. One or both terminals of antisense for miR-16 were linked with CL to prepare 5′3′CL-R16, 5′CL-R16, and 3′CL-R16 (Figure 6A), and these AMOs were assayed in HCT116 cells. 5′3′CL-R16, with CL at both termini, exhibited the highest activity, followed by 5′CL-R16. The activity of 3′CL-R16 did not reach the same level as that of 5′CL-R16 observed in AMOs targeting miR-21. Fold increases in hRluc/Fluc at 1.5 nM compared to the control without AMO (0 nM) of 5′3′CL-R16, 5′CL-R16, and 3′CL-R16 were 4.9, 3.3, and 2.3, respectively. We also confirmed that cross-linked hairpin-type AMO was more effective than the normal hairpin AMO (Figure 6B). In the assays for miR-16, AMO concentrations varied from 0 to 1.5 nM because the differences in anti-miRNA activities became more evident at low-AMO concentrations. This would be mainly the result of the low functional activity and narrow dynamic range of miR-16 in the dual luciferase assay (compare intensity in Figures 3A and 6A at 0 nM concentration) as previously reported.[31,41] Similar structural dependency was confirmed in AMOs targeting let-7c (Figure 6C). These results suggest that the structure-function relationship of the CL-AMOs might be derived from a common mechanism in the AMO-miRISC interaction.

CL-AMOs Show No Immune Activation

Single- or double-stranded DNAs and RNAs are recognized by Toll-like receptors in mammalian cells, resulting in significant toxic effects.[55] Although short MeRNA oligonucleotides are known not to have immune stimulatory action,[56] there has been no evidence for immune inactivation of the CL-modified MeRNAs. HeLa cells were transfected with 10 nM 5′3′CL, 5′CL, or 3′CL, and the mRNA levels of the interferon-responsive genes *OAS1*, *MX1*, *IRF9*, and *IFITM1* were evaluated at 7 and 24 hr post-transfection by qRT-PCR.[31] The results (Figure S11) clearly show that the CL-AMOs do not induce an immune response in cells as judged by the interferon induction level. We also confirmed no significant cytotoxicity of the CL-AMOs upon transfection by lactate dehydrogenase (LDH) assay (Figure S12).

DISCUSSION

Single-stranded guide RNA is incorporated into Ago protein, and the resulting Ago-guide complex plays a central role in si/miRISC. Crystallographic analyses of prokaryotic and eukaryotic Ago-guide complexes have revealed that both target and guide RNA are orderly positioned on four domains of Ago.[45,57–62] Ago-guide association to target RNA is primarily mediated via base paring at the seed region of the guide RNA, followed by propagation to the adjacent central and supplemental regions of guide[3,4] (top, Figure 7). This guide-target paring is reported to be blocked at the sixteenth nucleotide from the 5′ end of the guide by the N domain, which acts like a wedge in the RISC assembly process.[7] Hence, the 3′ tail of the guide is likely to remain as a single strand on Ago or weakly contact the target. This is consistent with previous results, which showed that Ago2-guide complex is able to tolerate mismatches opposite the 3′ tail region for its activity.[4,5,53]

In this study, we have employed cross-linked MeRNAs (CLs) to stabilize duplexes flanking a single-stranded AMO and have evaluated the function of the duplexes in inhibiting miRNAs, with two notable results. First, the inhibitory effect of single-stranded AMOs could be enhanced by linking with CL. Of AMOs tested here, AMO with CL at both terminals (5′3′CL) exhibited the highest inhibitory activity, with binding with the seed region found to be essential for 5′3′CL activity.

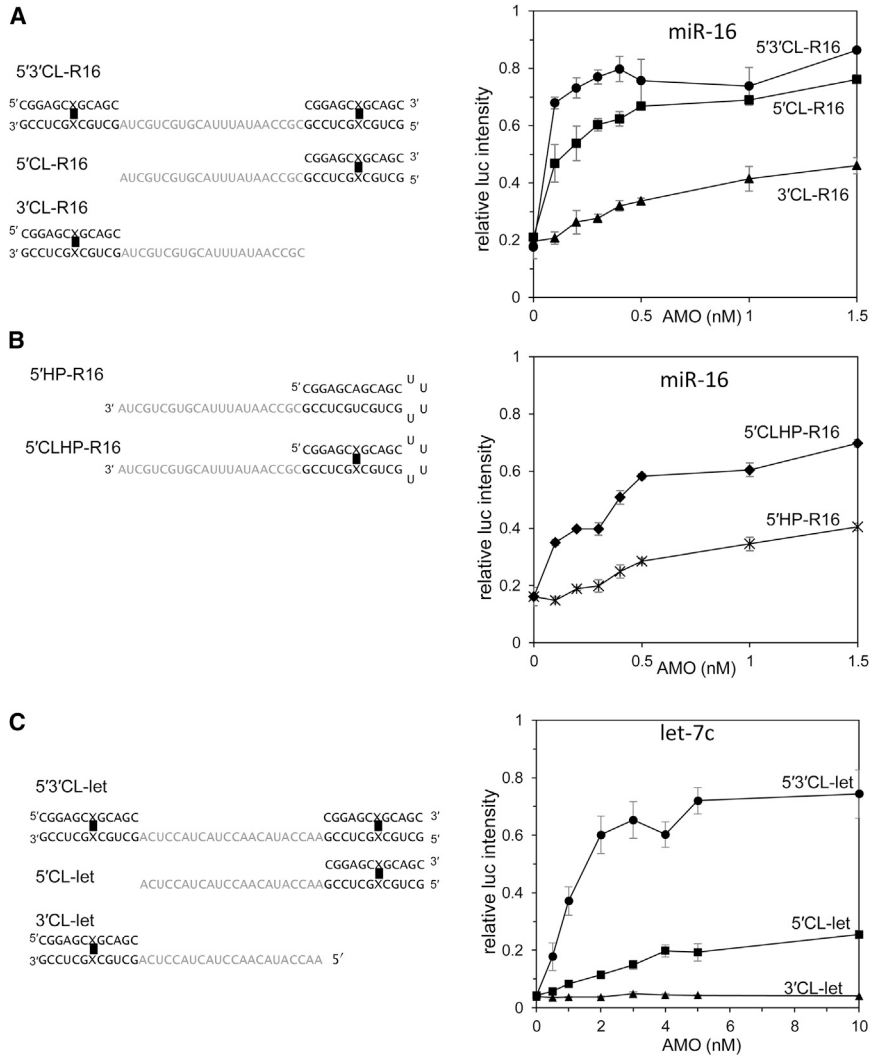

Figure 6. Generality of CL Effects on miRNA Inhibition of AMO

Sequences and inhibitory activities of AMOs flanked by CL at their 5′ and 3′, 5′, or 3′ position against miR-16 (A) and let-7c (C) and of AMOs flanked by the hairpin structure with and without cross-linking against miR-16 (B). Activities are represented by relative luciferase intensities 48 hr post-AMO transfection as mean ± SD (n = 3 independent experiments).

Thus, 5′3′CL could be recognized by the Ago-guide complex in the same manner as target RNAs. Second, AMOs with CLs at either the 5′ or 3′ terminal (5′CL, 3′CL) showed different results in anti-miRNA activity, nuclease resistance, and miRNA modification pattern. Interestingly, the 5′-side CL might play a more important role in anti-miRNA activity than the 3′-side CL.

When 5′3′CL or 5′CL, which contains CL on the 5′ side, binds the Ago-guide complex (left, Figure 7), the 5′ duplex approaches the N domain and sterically clashes with it following the propagation step. Note that the CL is not dissociated and has the potential to stabilize the adjacent hybridization due to a high stacking effect. Thus, the 5′-side CL might replace the N domain from the wedging position and promote the 3′ tail to stably bind the opposite, complementary AMO sequence (bottom, Figure 7). Interference with 3′-tail binding by incorporating a mismatch (5′CL-M) or by steric masking (5′CLsp-2) significantly reduced anti-miRNA activity (Figure 3B), supporting the notion that 3′-tail binding occurs in 5′3′CL and 5′CL. Interestingly, the insertion of a spacer between the 5′ duplex and the antisense region decreased anti-miRNA activity (5′CLsp2, 5′CLsp5; Figure 3B). This can be explained by the failure in repositioning the N domain due to the presence of the flexible spacer or by a weakened stacking effect of the CL. Recently, the structure of silkworm P-element induced wimpy testis (PIWI)-clade Ago (Siwi) complexed with PIWI-interacting RNA (piRNA) has been solved and revealed that the alignment of the N-PAZ lobes with respect to the MID-PIWI lobes differs from that of human Ago (hAgo).[63] This distortion of the N-PAZ lobes allows the 3′ tail of piRNA to form a duplex with target RNA. Similar structural changes of the N-PAZ domains might be induced upon binding with the 5′ side CL of AMOs.

On the other hand, 3′CL is expected not to interfere with the N domain because of the lack of the 5′-side CL (Figure 7, right). Hence, 3′CL acted like a single-stranded AMO in guide-strand modification (Figure 5A) and provided a less-stable Ago-guide-AMO complex than 5′CL, as observed in IP analyses (Figure 5C). However, 3′CL importantly showed high nuclease resistance, which is attributed to the extra stable CL structure on the 3′ side. Thus, the 3′-side CL contributes to the higher activity of 5′3′CL through cooperative functions with the 5′-side CL. We improved the 3′-exonuclease resistance of 5′CL by introducing phosphorothioate linkage into the 3′ end (5′CLps; Figure 4B), and 5′CLps was observed to increase anti-miRNA activity; however, 5′CLps was still less active than 5′3′CL. The difference in activity between 5′3′CL and 5′CLps suggests that the 3′-side duplex may have another role in inhibitory activity.

Finally, the stable and indissociable cross-linked duplex structure was found to be useful in enhancing the miRNA inhibition activity of AMOs and also in revealing the underlying mechanism of biological events in which duplex structures interact, confirming its significance and potential in functional oligonucleotides. The results described indicate that rational molecular designs of AMOs are possible in controlling miRNA functions.

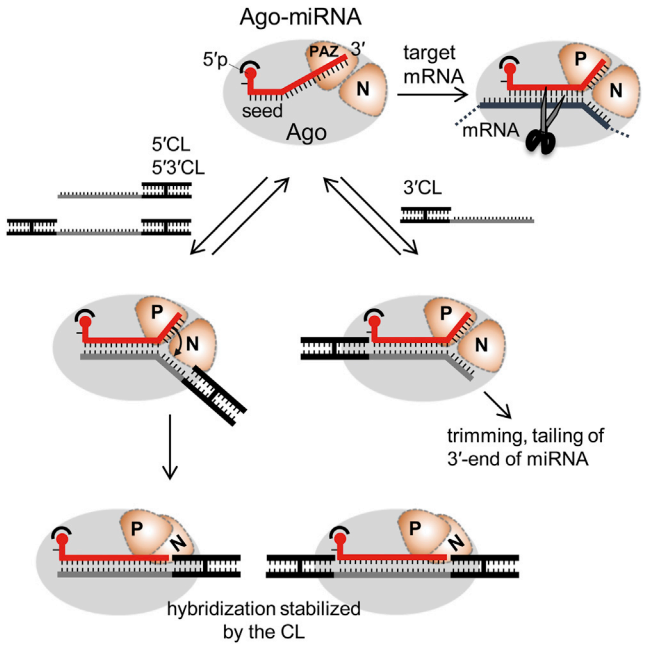

Figure 7. Schematic Representation of miRISC Inhibition by AMO with (Left) and without (Right) Hybridization at the miRNA 3′ End Region, Promoted by the Introduced CL Structure

P and N indicate PAZ (P) and N domain, respectively. MiRNA and CL-AMOs are shown in red and black + gray, respectively. The 5′-phosphate group of miRNA is shown in red circle (5′p).

MATERIALS AND METHODS

AMOs

MiRNA hairpin inhibitor-miR-21 was purchased from Thermo Scientific (miRIDIAN microRNA hairpin inhibitors, IH-300492-05). Anti-miR-21-5p tough decoy RNA was purchased from Sigma-Aldrich (MISSION Synthetic microRNA Inhibitor).

Preparation of MeRNA AMOs Containing Interstrand Cross-Link Sites

All MeRNAs containing deoxyuridine were chemically synthesized using standard phosphoramidite chemistry. Cleavage of MeRNAs from the controlled pore glass and deprotection of the protecting groups were carried out in AMA solution at 65°C for 10 min.[64] Cross-link reactions of MeRNAs were performed under the same condition as that for DNA duplexes.[37,39] The scheme and conditions of cross-link reactions for two- or three-stranded MeRNAs are described in Figure S1.

CD Measurements

Cross-linked and perfect-match duplexes (CL12, DS12) were dissolved in the solution (300 μL; 3 μM) containing 50 mM sodium phosphate buffer (pH 7) and 10 mM NaCl. CD measurements were performed using a 1 mm path length cell and wavelengths were scanned from 350 nm to 200 nm (J-820, JASCO). CD spectra were determined from the integration of five scan data. Molecular ellipticities of 265 nm were also measured at each temperature, which was increased from 25°C to 85°C at the rate of 1°C/min.

Tm Measurements

Thermal denaturation experiments of all duplexes (1.0 μM) were carried out in 10 mM sodium cacodylate buffer (pH 7) containing 10 mM NaCl. The solutions were heated at 90°C for 3 min, gradually cooled to anneal each duplex. UV absorbance of these duplexes was measured by the use of UV-2500PC (Shimadzu), and Tm values were calculated from their plots.

Cell Culture and Luciferase Assays

HeLa cells were cultured in DMEM (Sigma) supplemented with 10% fetal bovine serum (FBS; GIBCO), 100 U/mL penicillin (Gibco), and 100 μg/mL streptomycin (Gibco), respectively. A target sequence complementary to mature miR-21 was inserted into the 3′ UTR of the hRluc gene of the psiCHECK-2 vector (Promega) (*SgfI*/*PmeI* sites), yielding plasmid psiCHECK-2-miR21, which contained both hRluc and Fluc genes. HeLa cells were seeded at densities of 2×10^4 cells per well in 96-well plates (Nunc) in DMEM (200 μL) containing 10% FBS the day before transfection. After an aliquot (100 μL) was removed from each well, the cells were transfected in triplicate with DMEM solution (10 μL) containing Lipofectamine 2000 (Invitrogen; 0.3 μL per well), psiCHECK-2-miR21 (100 ng per well), and AMOs. The concentrations of AMOs were varied from 0 to 10 nM (up to 35 nM for 5′CL and 3′CL). Luciferase activity measurements were performed at 48 hr post-transfection according to the manufacturer's instructions (Promega, Dual-Glo Luciferase Assay System). The ratios of hRluc to Fluc (hRluc/Fluc) were first calculated from the average of triplicate wells. Then, all ratios were normalized using the ratio of psiCHECK-2-treated cells without AMO.

Nuclease Resistance

AMOs (5′3′CL, 5′CL, 3′CL; 25 pmol) were dissolved in the snake venom phosphodiesterase (SVPD) digestion buffer (25 μL) containing 50 mM Tris-HCl (pH 8), 10 mM $MgCl_2$, and incubated with SVPD (0.4 μg) at 37°C. After specified time intervals, an aliquot (4 μL) was removed from the reaction solution, then transferred into the gel loading solution (4 μL) containing 50 mM EDTA, 10 M urea to stop the nuclease reaction. After the reaction products were analyzed with 20% PAGE containing 8 M urea, the gel was stained with SYBR Gold (Thermo Scientific).

Real-Time Bioluminescence Monitoring

HeLa cells were seeded in 24-well black clear-bottom plates (Nunc) at 1×10^5 cells per well 1 day before transfection. HeLa cells were cotransfected with reporter plasmids, pSV40-SLG-PEST carrying miR-21 binding sequence at the 3′ UTR of the green-emitting SLG gene (*XbaI*/*FseI* site) (125 ng per well), pTK-SLR3 as an internal control vector (375 ng per well), and 2 nM of AMOs using Lipofectamine 2000 (Invitrogen) according to the manufacturer's instructions. One day after the transfection, the culture medium was replaced with DMEM without phenol red supplemented with 10% FBS, 25 mM HEPES/NaOH (pH 7.0; Sigma-Aldrich), 200 μM D-luciferin

potassium salt (RESEM, Lijnden, the Netherlands). Bioluminescence was measured and calculated as reported previously.[46,47] In brief, bioluminescence was recorded for 5 s at intervals of 10 min in the absence or presence of the R62 long-pass filter (HOYA, Tokyo, Japan) under a humidified atmosphere containing 5% CO_2 at 37°C using a microplate-type luminometer (WSL-1560, ATTO, Tokyo, Japan).

Immunoprecipitation of Ago2 and RNA Blot

Immunoprecipitation of Ago2 complex from HeLa cells transfected with AMO was conducted using the 4G8 anti-Ago2 antibody and miRNA isolation kit (Wako) according to the manufacture's instructions. The obtained sample was electrophoresed using 15% polyacrylamide gel containing 8 M urea. Oligonucleotides were transferred to positively charged nylon membrane (Roche) and UV cross-linked. A digoxigenin (DIG)-linked deoxyoligonucleotide probe for AMO-complementary sequence was prepared using DIG-tailing kit (Roche) and subjected to hybridization with AMO on the membrane. The membrane was then washed with 2× and 0.5× saline-sodium citrate (SSC) with 0.1% SDS. Detection was performed with Lumino Graph (ATTO) using a DIG luminescent detection kit (Roche). Northern blot analysis of miR-21 in HeLa cells transfected with AMO was carried out after total RNA isolation using miRNeasy Mini Kit (QIAGEN). Denatured PAGE was then conducted using gel containing 20% formamide and 8 M urea. We confirmed that miR-21 and AMO were separated in the denaturing PAGE, which did not interfere with miR-21 detection.[52,54] A DIG-tailed deoxyoligonucleotide probe complementary to the miR-21 was used for detection.

qRT-PCR of mRNAs for hRluc Gene with miR-21 Complimentary Sequence and Interferon Responsive Genes

HeLa cells were seeded in 96-well plates 1 day prior to transfection. Cells were transfected with the dual luciferase plasmid with a perfect-match target site for miR-21 at the 3′ UTR of hRluc gene and with/without 5 nM AMO using Lipofectamine 2000. Total RNA was isolated 48 hr post-transcription and treated with DNase I (QIAGEN) to remove DNA contamination. The obtained RNA was reverse transcribed into cDNA using the SuperScript III First-Strand Synthesis System (Thermo Scientific) with oligo$(dT)_{20}$ primer. Real-time PCR was performed using Platinum SYBR green qPCR Supermix (Thermo Scientific). Relative mRNA levels of hRluc with miR-21 binding sequence (miR-21BS) at its 3′ region was calculated by the ΔΔCt method using Fluc mRNA level for normalization. Primer sequences for Renilla-miR-21BS were 5′-GAGGACGCTC CAGATGAAATG-3′ (forward) and 5′-GGCCGCTCTAGGTTTAA ACTAG-3′ (reverse), and those for Fluc were 5′-CGTGCCAG AGTCTTTCGACA-3′ (forward) and 5′-ACAGGCGGTGCGAT GAG-3′ (reverse), according to the literature.[65] Immune response analysis were carried out according to the previous report[31] with 0 and 10 nM AMO without plasmid.

SUPPLEMENTAL INFORMATION

Supplemental Information includes Supplemental Materials and Methods and twelve figures and can be found with this article online at https://doi.org/10.1016/j.omtn.2017.11.003.

AUTHOR CONTRIBUTIONS

Conceptualization, Y.K.; Investigation, Y.M., Y.H., K.K., A.N., M.Y., Y.N., Y.K.; Writing – Original Draft, Y.M., Y.H., Y.K.; Writing – Review & Editing, Y.M., Y.H., A.N., Y.N., Y.K.; Funding Acquisition, Y.M., Y.N., Y.K.; Supervision, Y.K.

ACKNOWLEDGMENTS

We thank Dr. Eiko Ohtsuka for helpful discussion. This work was supported by the Ministry of Education, Culture, Sports, Science and Technology, Japan (Grant-in-Aid for Scientific Research 25293030, 16H05106, 16K08218, and 16H03295).

REFERENCES

1. Kobayashi, H., and Tomari, Y. (2016). RISC assembly: coordination between small RNAs and Argonaute proteins. Biochim. Biophys. Acta *1859*, 71–81.
2. Stroynowska-Czerwinska, A., Fiszer, A., and Krzyzosiak, W.J. (2014). The panorama of miRNA-mediated mechanisms in mammalian cells. Cell. Mol. Life Sci. *71*, 2253–2270.
3. Bartel, D.P. (2009). MicroRNAs: target recognition and regulatory functions. Cell *136*, 215–233.
4. Wee, L.M., Flores-Jasso, C.F., Salomon, W.E., and Zamore, P.D. (2012). Argonaute divides its RNA guide into domains with distinct functions and RNA-binding properties. Cell *151*, 1055–1067.
5. Jo, M.H., Shin, S., Jung, S.R., Kim, E., Song, J.J., and Hohng, S. (2015). Human argonaute 2 has diverse reaction pathways on target RNAs. Mol. Cell *59*, 117–124.
6. Ameres, S.L., Martinez, J., and Schroeder, R. (2007). Molecular basis for target RNA recognition and cleavage by human RISC. Cell *130*, 101–112.
7. Kwak, P.B., and Tomari, Y. (2012). The N domain of Argonaute drives duplex unwinding during RISC assembly. Nat. Struct. Mol. Biol. *19*, 145–151.
8. Thomson, D.W., and Dinger, M.E. (2016). Endogenous microRNA sponges: evidence and controversy. Nat. Rev. Genet. *17*, 272–283.
9. Freiesleben, S., Hecker, M., Zettl, U.K., Fuellen, G., and Taher, L. (2016). Analysis of microRNA and gene expression profiles in multiple sclerosis: integrating interaction data to uncover regulatory mechanisms. Sci. Rep. *6*, 34512.
10. Memczak, S., Jens, M., Elefsinioti, A., Torti, F., Krueger, J., Rybak, A., Maier, L., Mackowiak, S.D., Gregersen, L.H., Munschauer, M., et al. (2013). Circular RNAs are a large class of animal RNAs with regulatory potency. Nature *495*, 333–338.
11. Hansen, T.B., Jensen, T.I., Clausen, B.H., Bramsen, J.B., Finsen, B., Damgaard, C.K., and Kjems, J. (2013). Natural RNA circles function as efficient microRNA sponges. Nature *495*, 384–388.
12. Ventura, A., and Jacks, T. (2009). MicroRNAs and cancer: short RNAs go a long way. Cell *136*, 586–591.
13. Rayner, K.J., Suárez, Y., Dávalos, A., Parathath, S., Fitzgerald, M.L., Tamehiro, N., Fisher, E.A., Moore, K.J., and Fernández-Hernando, C. (2010). MiR-33 contributes to the regulation of cholesterol homeostasis. Science *328*, 1570–1573.
14. van Rooij, E., and Olson, E.N. (2012). MicroRNA therapeutics for cardiovascular disease: opportunities and obstacles. Nat. Rev. Drug Discov. *11*, 860–872.
15. van Rooij, E., and Kauppinen, S. (2014). Development of microRNA therapeutics is coming of age. EMBO Mol. Med. *6*, 851–864.
16. Gambari, R., Brognara, E., Spandidos, D.A., and Fabbri, E. (2016). Targeting oncomiRNAs and mimicking tumor suppressor miRNAs: vew trends in the development of miRNA therapeutic strategies in oncology (Review). Int. J. Oncol. *49*, 5–32.
17. Hayes, J., Peruzzi, P.P., and Lawler, S. (2014). MicroRNAs in cancer: biomarkers, functions and therapy. Trends Mol. Med. *20*, 460–469.
18. Kosaka, N., Yoshioka, Y., Fujita, Y., and Ochiya, T. (2016). Versatile roles of extracellular vesicles in cancer. J. Clin. Invest. *126*, 1163–1172.

19. Obad, S., dos Santos, C.O., Petri, A., Heidenblad, M., Broom, O., Ruse, C., Fu, C., Lindow, M., Stenvang, J., Straarup, E.M., et al. (2011). Silencing of microRNA families by seed-targeting tiny LNAs. Nat. Genet. *43*, 371–378.

20. Lennox, K.A., and Behlke, M.A. (2011). Chemical modification and design of anti-miRNA oligonucleotides. Gene Ther. *18*, 1111–1120.

21. Davis, S., Lollo, B., Freier, S., and Esau, C. (2006). Improved targeting of miRNA with antisense oligonucleotides. Nucleic Acids Res. *34*, 2294–2304.

22. Krützfeldt, J., Kuwajima, S., Braich, R., Rajeev, K.G., Pena, J., Tuschl, T., Manoharan, M., and Stoffel, M. (2007). Specificity, duplex degradation and subcellular localization of antagomirs. Nucleic Acids Res. *35*, 2885–2892.

23. Kloosterman, W.P., Lagendijk, A.K., Ketting, R.F., Moulton, J.D., and Plasterk, R.H.A. (2007). Targeted inhibition of miRNA maturation with morpholinos reveals a role for miR-375 in pancreatic islet development. PLoS Biol. *5*, e203.

24. Fabani, M.M., and Gait, M.J. (2008). miR-122 targeting with LNA/2′-O-methyl oligonucleotide mixmers, peptide nucleic acids (PNA), and PNA-peptide conjugates. RNA *14*, 336–346.

25. Cheng, C.J., Bahal, R., Babar, I.A., Pincus, Z., Barrera, F., Liu, C., Svoronos, A., Braddock, D.T., Glazer, P.M., Engelman, D.M., et al. (2015). MicroRNA silencing for cancer therapy targeted to the tumour microenvironment. Nature *518*, 107–110.

26. Scherr, M., Venturini, L., Battmer, K., Schaller-Schoenitz, M., Schaefer, D., Dallmann, I., Ganser, A., and Eder, M. (2007). Lentivirus-mediated antagomir expression for specific inhibition of miRNA function. Nucleic Acids Res. *35*, e149.

27. Ebert, M.S., Neilson, J.R., and Sharp, P.A. (2007). MicroRNA sponges: competitive inhibitors of small RNAs in mammalian cells. Nat. Methods *4*, 721–726.

28. Sayed, D., Rane, S., Lypowy, J., He, M., Chen, I.Y., Vashistha, H., Yan, L., Malhotra, A., Vatner, D., and Abdellatif, M. (2008). MicroRNA-21 targets Sprouty2 and promotes cellular outgrowths. Mol. Biol. Cell *19*, 3272–3282.

29. Haraguchi, T., Ozaki, Y., and Iba, H. (2009). Vectors expressing efficient RNA decoys achieve the long-term suppression of specific microRNA activity in mammalian cells. Nucleic Acids Res. *37*, e43.

30. Cao, H., Yu, W., Li, X., Wang, J., Gao, S., Holton, N.E., Eliason, S., Sharp, T., and Amendt, B.A. (2016). A new plasmid-based microRNA inhibitor system that inhibits microRNA families in transgenic mice and cells: a potential new therapeutic reagent. Gene Ther. *23*, 527–542.

31. Haraguchi, T., Nakano, H., Tagawa, T., Ohki, T., Ueno, Y., Yoshida, T., and Iba, H. (2012). A potent 2′-O-methylated RNA-based microRNA inhibitor with unique secondary structures. Nucleic Acids Res. *40*, e58.

32. Vermeulen, A., Robertson, B., Dalby, A.B., Marshall, W.S., Karpilow, J., Leake, D., Khvorova, A., and Baskerville, S. (2007). Double-stranded regions are essential design components of potent inhibitors of RISC function. RNA *13*, 723–730.

33. Robertson, B., Dalby, A.B., Karpilow, J., Khvorova, A., Leake, D., and Vermeulen, A. (2010). Specificity and functionality of microRNA inhibitors. Silence *1*, 10.

34. Nakano, S., Miyoshi, D., and Sugimoto, N. (2014). Effects of molecular crowding on the structures, interactions, and functions of nucleic acids. Chem. Rev. *114*, 2733–2758.

35. Carrette, L.L.G., Gyssels, E., De Laet, N., and Madder, A. (2016). Furan oxidation based cross-linking: a new approach for the study and targeting of nucleic acid and protein interactions. Chem. Commun. (Camb.) *52*, 1539–1554.

36. Onizuka, K., Hazemi, M.E., Thomas, J.M., Monteleone, L.R., Yamada, K., Imoto, S., Beal, P.A., and Nagatsugi, F. (2017). Synthesis of native-like crosslinked duplex RNA and study of its properties. Bioorg. Med. Chem. *25*, 2191–2199.

37. Ichikawa, K., Kojima, N., Hirano, Y., Takebayashi, T., Kowata, K., and Komatsu, Y. (2012). Interstrand cross-link of DNA by covalently linking a pair of abasic sites. Chem. Commun. (Camb.) *48*, 2143–2145.

38. Yasuhiro, M., Naoshi, K., Keiko, K., and Yasuo, K. (2012). End-tether structure of DNA alters electron-transfer pathway of redox-labeled oligo-DNA duplex at electrode surface. Chem. Lett. *41*, 62–64.

39. Hirano, Y., Ikegami, M., Kowata, K., and Komatsu, Y. (2017). Bienzyme reactions on cross-linked DNA scaffolds for electrochemical analysis. Bioelectrochemistry *113*, 15–19.

40. Fujii, N., Evison, B.J., Actis, M.L., and Inoue, A. (2015). A novel assay revealed that ribonucleotide reductase is functionally important for interstrand DNA crosslink repair. Bioorg. Med. Chem. *23*, 6912–6921.

41. Lennox, K.A., and Behlke, M.A. (2010). A direct comparison of anti-microRNA oligonucleotide potency. Pharm. Res. *27*, 1788–1799.

42. Lennox, K.A., Owczarzy, R., Thomas, D.M., Walder, J.A., and Behlke, M.A. (2013). Improved performance of anti-miRNA oligonucleotides using a novel non-nucleotide modifier. Mol. Ther. Nucleic Acids *2*, e117.

43. Liu, J., Carmell, M.A., Rivas, F.V., Marsden, C.G., Thomson, J.M., Song, J.J., Hammond, S.M., Joshua-Tor, L., and Hannon, G.J. (2004). Argonaute2 is the catalytic engine of mammalian RNAi. Science *305*, 1437–1441.

44. Jonas, S., and Izaurralde, E. (2015). Towards a molecular understanding of microRNA-mediated gene silencing. Nat. Rev. Genet. *16*, 421–433.

45. Schirle, N.T., Sheu-Gruttadauria, J., and MacRae, I.J. (2014). Structural basis for microRNA targeting. Science *346*, 608–613.

46. Noguchi, T., Michihata, T., Nakamura, W., Takumi, T., Shimizu, R., Yamamoto, M., Ikeda, M., Ohmiya, Y., and Nakajima, Y. (2010). Dual-color luciferase mouse directly demonstrates coupled expression of two clock genes. Biochemistry *49*, 8053–8061.

47. Noguchi, T., Ikeda, M., Ohmiya, Y., and Nakajima, Y. (2012). A dual-color luciferase assay system reveals circadian resetting of cultured fibroblasts by co-cultured adrenal glands. PLoS ONE *7*, e37093.

48. Zhang, J.G., Wang, J.J., Zhao, F., Liu, Q., Jiang, K., and Yang, G.H. (2010). MicroRNA-21 (miR-21) represses tumor suppressor PTEN and promotes growth and invasion in non-small cell lung cancer (NSCLC). Clin. Chim. Acta *411*, 846–852.

49. Boele, J., Persson, H., Shin, J.W., Ishizu, Y., Newie, I.S., Søkilde, R., Hawkins, S.M., Coarfa, C., Ikeda, K., Takayama, K., et al. (2014). PAPD5-mediated 3′ adenylation and subsequent degradation of miR-21 is disrupted in proliferative disease. Proc. Natl. Acad. Sci. USA *111*, 11467–11472.

50. Ameres, S.L., Horwich, M.D., Hung, J.H., Xu, J., Ghildiyal, M., Weng, Z., and Zamore, P.D. (2010). Target RNA-directed trimming and tailing of small silencing RNAs. Science *328*, 1534–1539.

51. Haas, G., Cetin, S., Messmer, M., Chane-Woon-Ming, B., Terenzi, O., Chicher, J., Kuhn, L., Hammann, P., and Pfeffer, S. (2016). Identification of factors involved in target RNA-directed microRNA degradation. Nucleic Acids Res. *44*, 2873–2887.

52. Torres, A.G., Fabani, M.M., Vigorito, E., and Gait, M.J. (2011). MicroRNA fate upon targeting with anti-miRNA oligonucleotides as revealed by an improved Northern-blot-based method for miRNA detection. RNA *17*, 933–943.

53. Hogan, D.J., Vincent, T.M., Fish, S., Marcusson, E.G., Bhat, B., Chau, B.N., and Zisoulis, D.G. (2014). Anti-miRs competitively inhibit microRNAs in Argonaute complexes. PLoS ONE *9*, e100951.

54. Davis, S., Propp, S., Freier, S.M., Jones, L.E., Serra, M.J., Kinberger, G., Bhat, B., Swayze, E.E., Bennett, C.F., and Esau, C. (2009). Potent inhibition of microRNA in vivo without degradation. Nucleic Acids Res. *37*, 70–77.

55. Akira, S., Uematsu, S., and Takeuchi, O. (2006). Pathogen recognition and innate immunity. Cell *124*, 783–801.

56. Robbins, M., Judge, A., Liang, L., McClintock, K., Yaworski, E., and MacLachlan, I. (2007). 2′-O-methyl-modified RNAs act as TLR7 antagonists. Mol. Ther. *15*, 1663–1669.

57. Wang, Y., Juranek, S., Li, H., Sheng, G., Wardle, G.S., Tuschl, T., and Patel, D.J. (2009). Nucleation, propagation and cleavage of target RNAs in Ago silencing complexes. Nature *461*, 754–761.

58. Miyoshi, T., Ito, K., Murakami, R., and Uchiumi, T. (2016). Structural basis for the recognition of guide RNA and target DNA heteroduplex by Argonaute. Nat. Commun. *7*, 11846.

59. Schirle, N.T., and MacRae, I.J. (2012). The crystal structure of human Argonaute2. Science *336*, 1037–1040.

60. Kuhn, C.D., and Joshua-Tor, L. (2013). Eukaryotic Argonautes come into focus. Trends Biochem. Sci. *38*, 263–271.

61. Elkayam, E., Kuhn, C.D., Tocilj, A., Haase, A.D., Greene, E.M., Hannon, G.J., and Joshua-Tor, L. (2012). The structure of human argonaute-2 in complex with miR-20a. Cell *150*, 100–110.

62. Nakanishi, K., Weinberg, D.E., Bartel, D.P., and Patel, D.J. (2012). Structure of yeast Argonaute with guide RNA. Nature *486*, 368–374.

63. Matsumoto, N., Nishimasu, H., Sakakibara, K., Nishida, K.M., Hirano, T., Ishitani, R., Siomi, H., Siomi, M.C., and Nureki, O. (2016). Crystal structure of silkworm PIWI-clade argonaute siwi bound to piRNA. Cell *167*, 484–497.e9.

64. Kowata, K., Kojima, N., and Komatsu, Y. (2016). Development of a 3′-amino linker with high conjugation activity and its application to conveniently cross-link blunt ends of a duplex. Bioorg. Med. Chem. *24*, 2108–2113.

65. Lin, J., Lwin, T., Zhao, J.J., Tam, W., Choi, Y.S., Moscinski, L.C., Dalton, W.S., Sotomayor, E.M., Wright, K.L., and Tao, J. (2011). Follicular dendritic cell-induced microRNA-mediated upregulation of PRDM1 and downregulation of BCL-6 in non-Hodgkin's B-cell lymphomas. Leukemia *25*, 145–152.